24th COBEM - 2017

24th ABCM International Congress of Mechanical Engineering
December 3-8, 2017, Curitiba, PR, Brazil

COBEM-2017-1025
WSGG CORRELATIONS FOR H_2O AND CO_2 IN HIGH PRESSURE CONDITIONS

Felipe Ramos Coelho
Francis Henrique Ramos França
Universidade Federal do Rio Grande do Sul, Department of Mechanical Engineering, Av. Paulo Gama, 110, Porto Alegre, RS, Brazil
felipe.coelho@ufrgs.br
frfranca@mecanica.ufrgs.br

Abstract. *Thermal radiation is often a very important heat transfer mechanism in high pressure combustion processes due to the presence of participating media and the high temperatures involved. Solving thermal radiation in participating media is a tough problem due to the integro-differential governing equation and the complex spectral dependence of radiation properties. Currently, the most accurate method to solve the spectral integration is the line-by-line (LBL) method, which has a very high computational cost. In order to avoid this drawback the spectral problem is usually solved using spectral models, and as a consequence the radiative transfer equation (RTE) is simplified. One of the models is the weighted-sum-of-gray-gases (WSGG) which replaces the highly irregular spectral behavior of the absorption coefficient by bands of uniform pressure absorption coefficients, and has shown great performance in a lot of applications even though it is a very simple model. However, recently some authors didn't have good results when trying to apply the WSGG to high pressure combustion problems. This paper develops a WSGG model for both CO_2 and H_2O on high pressure conditions. In order to validate the model the total emittance is calculated using the WSGG coefficients and compared to the LBL solution which was obtained using the HITEMP 2010 spectral emissivity database. The results showed that the emittance values from both methods were very close even for high pressure values for both CO_2 and H_2O proving that the WSGG method is applicable to high pressure conditions. A second validation was made through results of radiative heat flux and heat source and compared to the LBL solution with acceptable deviations. The effect of pressure on LBL solution showed that both radiative heat flux and heat source increased more than 100% from 1 atm to 10 atm, and more than 150% from 1 atm to 40 atm. The WSGG method presented lowest deviations for CO_2 at 40 atm proving that the method is accurate for CO_2 at high pressure values while for H_2O it presented an opposite behavior.*

Keywords: *Thermal radiation, weighted-sum-of-gray-gases, line-by-line, high pressures.*

1. INTRODUCTION

With increasing environmental restrictions, researchers have sought to increase efficiency and reduce emissions from combustion processes. A large share of combustion applications such as internal combustion engines and gas turbines operate at high pressures (Matynia *et al*., 2012; Charest *et al*., 2014). Another promising application of high pressure combustion is the use of oxy-fuel combustion to capture and store carbon, in order to reduce CO_2 emissions in the atmosphere (Wall *et al*., 2011).

Thermal radiation is often a very important form of heat exchange in combustion processes, due to its high temperatures involved and the generation of products that behave as participating gases. The radiative heat transfer energy balance on a participating media results in the radiative transfer equation (RTE) which is solved by spatial and spectral integration. The most accurate way to solve the RTE is through the line-by-line (LBL) method, which considers all the variations of the spectral properties along the spectrum, and thus has high computational cost. The spectral properties of the participant gas are usually taken from spectral databases such as HITEMP 2010 (Rothman *et al*., 2010).

However, some of the spectral properties have a highly irregular spectral dependence, and in order to simplify this problem and avoid the high computational cost of the LBL method, several spectral models were developed. The weighted-sum-of-gray-gases (WSGG) model, proposed by Hottel and Sarofim (1967), is an example of spectral model which replaces the original behavior of the absorption coefficient of a participating gas by a few equivalent gray gases with uniform pressure absorption coefficient. Smith et al., 1982, proposed a new methodology for obtaining WSGG

coefficients based on a polynomial fit of the weighting factors as a function of temperature, and generated new WSGG coefficients considering three gray gases. Using this same new methodology, Kangwanpongpan *et al*., 2012, generated new coefficients based on HITEMP 2010 database for oxy-fire combustion conditions. Dorigon *et al*., 2013, obtained WSGG coefficients considering four gray gases for a mixture composed of CO_2 and H_2O, at atmospheric pressure and for a wide range of applications. Cassol *et al*., 2014, obtained WSGG coefficients for single species of CO_2 and H_2O, and by using a superposition methodology were able to reproduce mixture results for non-isothermal, non-homogeneous, and non-fixed molar ratio conditions.

Some recent works attempt to apply the WSGG method for high pressures conditions. Bordbar *et al*., 2014, developed WSGG coefficients for oxy-fired combustion conditions for a wide range of temperature, pressure path-length, and molar ratios based on HITEMP 2010. These WSGG coefficients developed by Bordbar *et al*., 2014, were then used by Chu *et al.*, 2016, to solve an oxy-fuel combustion problem for total pressures ranging from 1 to 30 atm without success, especially between 1 and 10 atm. Kez *et al*., 2016, also solved an oxy-fuel combustion problem at 20 atm using the WSGG model from Bordbar *et al*., 2014, and had significant deviations, concluding that the WSGG model should not be applied for oxy-fuel combustion. Pearson *et al*., 2014, studied the effect of total pressure on the absorption spectrum from 0.1 atm to 50 atm, both using HITEMP 2010.

Based on these recent studies, this work seeks to develop a WSGG model applicable to high pressure conditions for both CO_2 and H_2O. To validate the model the total emittance is calculated by the WSGG coefficients and compared to other authors results and to the LBL solution, which is commonly regarded as the benchmark for spectral solutions.

2. METHODOLOGY

The energy balance for the radiative heat transfer in a participating media results in the RTE, and after neglecting the scattering effect it is given by (Siegel and Howell, 2002)

$$\frac{dI_\eta(x)}{dx} = -\kappa_\eta(x) I_\eta(x) + \kappa_\eta(x) I_{\eta b}(x) \tag{1}$$

in which κ_η is the absorption coefficient, in m^{-1}, and I_η and $I_{\eta b}$ represent the spectral intensity and the blackbody radiation intensity in $W/(m^2\ cm^{-1})$.

The absorption coefficient κ_η is calculated from

$$\kappa_\eta = NYC_\eta \tag{2}$$

The absorption cross-section is obtained from HITEMP 2010 database for molar fraction Y = 0.1 for CO_2 and Y = 0.2 for H_2O, temperatures ranging from 400 K to 2500 K, and total pressure values of 1 atm, 10 atm, and 40 atm. Molar fractions represents typical stoichiometric methane combustion (Dorigon *et al*., 2013; Cassol *et al*., 2014) and pressure range is the same as proposed by other authors (Pearson *et al*., 2014; Alberti *et al*., 2015).

Replacing the absorption coefficient κ_η by the absorption coefficient based on the pressure associated to each gray gas, $\kappa_{p,j}$, on Eq. (1) becomes

$$\frac{dI_j(x)}{dx} = -\kappa_{p,j} p_a(x) I_j(x) + \kappa_{p,j} p_a(x) a_j(T) I_b(T) \tag{3}$$

where p_a is the partial pressure, a_j is the temperature dependent coefficient, $I_b(T)$ is the total blackbody intensity.

The WSGG coefficients are then obtained by fitting the WSGG total emittance to the total emittance obtained by the line-by-line (LBL) method, which is given by

$$\varepsilon(T, p_a S) = \frac{\int_{\eta=0}^{\infty} I_{\eta b}(\eta, T)[1-\exp(-\kappa_{p\eta,a} p_a S)]d\eta}{\sigma T^4/\pi} \tag{4}$$

where $p_a S$ is the pressure path-length, and $I_{\eta b}$ is the blackbody intensity given by Planck's distribution. Applying Eq. (4) in the WSGG spectrum

$$\varepsilon(T, p_a S) = \sum_{j=1}^{J} a_j(T)[1-\exp(-\kappa_{p,j} p_a S)] \tag{5}$$

The coefficient $a_j(T)$ is the weighting factor for the j-th gray gas which is frequently fitted as a polynomial function of temperature as

$$a_j(T) = \sum_{k=0}^{K} b_{j,k} T^k \tag{6}$$

The total emittances are then calculated using Eq. (4) for the LBL and Eq. (5) for the WSGG with path-length ranging from 0,005 m $\leq S \leq$ 50 m, and same conditions as the previously obtained absorption cross-sections. This path-length range is close to the ones used by other authors (Smith *et al*., 1982; Kangwanpongpan *et al*., 2012; Dorigon *et al*., 2013; Cassol *et al*., 2014) and according to Smith *et al*., 1982, covers most practical engineering applications.

The WSGG model coefficients are fit from the total emittance values calculated by the LBL integration as shown on Eq. (4). The $\kappa_{p,j}$ and $a_j(T)$ coefficients are then obtained through Eq. (5) while the $b_{j,k}$ coefficients are determined from Eq. (6). The coefficients are then validated through a comparison between the WSGG emittance values calculated from Eq. (5) and the LBL emittance values which were used for the correlation.

As a second form of validation, the WSGG model results for radiative heat flux and heat source are compared with the LBL solution, for the problem of two infinite parallel walls with participating media between them. The walls are 1 m apart from each other and are considered as black bodies. The participating media is composed of either CO_2 with molar fraction of Y = 0.1 or H_2O with molar fraction of Y = 0.1, and with a temperature profile given by Eq. (7) which is the same used by Cassol *et al*., 2014.

$$T(x) = 400K + (1400K)\sin^2(\pi x) \tag{7}$$

The radiative heat flux $q_R^{"}$ and heat source S_R obtained by the LBL method are calculated by Eqs. (8) and (9), while for the WSGG method they are calculated through Eqs. (10) and (11).

$$q_R^{"}(x) = \sum_{m=1}^{n_d} \int 2\pi\mu_m\omega_m \left[I_{\eta,m}^{+}(x) - I_{\eta,m}^{-}(x) \right] d\eta \tag{8}$$

$$S_R(x) = \sum_{m=1}^{n_d} \int_{\eta} \left\{ 2\pi\kappa_\eta\omega_m \left[I_{\eta,m}^{+}(x) + I_{\eta,m}^{-}(x) \right] - 4\pi\kappa_\eta I_{\eta b} \right\} d\eta \tag{9}$$

$$q_R^{"}(x) = \sum_{m=1}^{n_d} \sum_{j=1}^{n_g} 2\pi\mu_m\omega_m \left[I_{j,m}^{+}(x) - I_{j,m}^{-}(x) \right] \tag{10}$$

$$S_R(x) = \sum_{m=1}^{n_d} \sum_{j=1}^{n_g} \left\{ 2\pi\omega_m\kappa_j \left[I_{j,m}^{+}(x) + I_{j,m}^{-}(x) \right] - 4\pi\kappa_j a_j I_{\eta b} \right\} \tag{11}$$

On the LBL formulation μ_m is the direction cosine in m direction, ω_m is the quadrature weight for m direction, and $I_{\eta,m}^{+}$ and $I_{\eta,m}^{-}$ are the radiative intensities for $\mu_m > 0$ e $\mu_m < 0$, respectively. Since the walls are considered as black bodies, the boundary conditions in x = 0 and $x = L$ are $I_{\eta,m}^{+}(0) = I_{\eta b}(0)$ and $I_{\eta,m}^{-}(L) = I_{\eta b}(L)$. For the WSGG, $I_{j,m}^{+}$ and $I_{j,m}^{-}$ are the radiation intensities for gray gas j for $\mu_m > 0$ and $\mu_m < 0$, respectively. The boundary conditions for x = 0 and x = L are $I_{j,m}^{+}(0) = a_j(0) I_{\eta b}(0)$ e $I_{j,m}^{-}(L) = a_j(L) I_{\eta b}(L)$.

3. RESULTS

The WSGG model coefficients for CO_2 are presented on Tables 1, 2, and 3 for total pressures of 1 atm, 10 atm, and 40 atm, respectively. The coefficients are valid for temperatures ranging from 400 K to 2500 K, path-lengths from 0.005 m to 50 m and molar fraction Y = 0.1.

Table 1 – WSGG model coefficients for CO_2 at total pressure of 1 atm.

j	$\kappa_{p,j}$ (atm m)$^{-1}$	$b_{j,0}$	$b_{j,1}$ (K^{-1})	$b_{j,2}$ (K^{-2})	$b_{j,3}$ (K^{-3})	$b_{j,4}$ (K^{-4})
1	0.261	2.442×10^{-2}	6.183×10^{-4}	-7.486×10^{-7}	3.335×10^{-10}	-5.198×10^{-14}
2	3.441	6.953×10^{-2}	-1.339×10^{-4}	2.582×10^{-7}	-1.481×10^{-10}	2.599×10^{-14}
3	25.691	1.102×10^{-1}	-2.044×10^{-4}	2.296×10^{-7}	-1.105×10^{-10}	1.817×10^{-14}
4	309.289	-4.009×10^{-2}	2.737×10^{-4}	-2.829×10^{-7}	1.097×10^{-10}	-1.491×10^{-14}

Table 2 – WSGG model coefficients for CO_2 at total pressure of 10 atm.

j	$\kappa_{p,j}$ (atm m)$^{-1}$	$b_{j,0}$	$b_{j,1}$ (K^{-1})	$b_{j,2}$ (K^{-2})	$b_{j,3}$ (K^{-3})	$b_{j,4}$ (K^{-4})
1	0.045	7.567×10^{-1}	-1.931×10^{-3}	2.233×10^{-6}	-1.030×10^{-9}	1.632×10^{-13}
2	0.374	2.455×10^{-2}	8.742×10^{-4}	-1.200×10^{-6}	5.665×10^{-10}	-9.037×10^{-14}
3	5.217	1.070×10^{-1}	-1.425×10^{-4}	2.505×10^{-7}	-1.435×10^{-10}	2.525×10^{-14}
4	151.891	5.294×10^{-2}	9.748×10^{-5}	-1.124×10^{-7}	3.459×10^{-11}	-3.061×10^{-15}

Table 3 – WSGG model coefficients for CO_2 at total pressure of 40 atm.

j	$\kappa_{p,j}$ (atm m)$^{-1}$	$b_{j,0}$	$b_{j,1}$ (K^{-1})	$b_{j,2}$ (K^{-2})	$b_{j,3}$ (K^{-3})	$b_{j,4}$ (K^{-4})
1	0.011	5.185×10^{-2}	-1.082×10^{-4}	4.682×10^{-7}	-2.774×10^{-10}	4.658×10^{-14}
2	0.175	5.762×10^{-1}	-1.065×10^{-3}	1.114×10^{-6}	-5.083×10^{-10}	8.096×10^{-14}
3	2.133	1.122×10^{-1}	4.491×10^{-4}	-6.088×10^{-7}	2.673×10^{-10}	-3.985×10^{-14}
4	58.250	1.244×10^{-1}	-4.333×10^{-5}	3.704×10^{-8}	-3.141×10^{-11}	6.992×10^{-15}

The WSGG model coefficients for H_2O however are valid for a molar fraction of $Y = 0.2$, for the same temperature and path-length ranges and are presented on Tables 4, 5, and 6 for total pressures of 1 atm, 10 atm, and 40 atm, respectively. Both the CO_2 and H_2O WSGG coefficients for total pressure of 1 atm are similar to the ones previously obtained by other authors, like the ones obtained by Cassol *et al*., 2014.

Table 4 – WSGG model coefficients for H_2O at total pressure of 1 atm.

j	$\kappa_{p,j}$ (atm m)$^{-1}$	$b_{j,0}$	$b_{j,1}$ (K^{-1})	$b_{j,2}$ (K^{-2})	$b_{j,3}$ (K^{-3})	$b_{j,4}$ (K^{-4})
1	0.182	8.998×10^{-2}	4.567×10^{-4}	-3.369×10^{-7}	1.510×10^{-10}	-2.723×10^{-14}
2	1.358	6.831×10^{-2}	2.308×10^{-4}	-2.674×10^{-9}	-7.251×10^{-11}	1.719×10^{-14}
3	7.819	3.448×10^{-4}	6.119×10^{-4}	-6.886×10^{-7}	2.789×10^{-10}	-3.980×10^{-14}
4	75.164	2.203×10^{-1}	-3.131×10^{-4}	1.741×10^{-7}	-4.492×10^{-11}	4.552×10^{-15}

Table 5 – WSGG model coefficients for H_2O at total pressure of 10 atm.

j	$\kappa_{p,j}$ (atm m)$^{-1}$	$b_{j,0}$	$b_{j,1}$ (K^{-1})	$b_{j,2}$ (K^{-2})	$b_{j,3}$ (K^{-3})	$b_{j,4}$ (K^{-4})
1	0.036	6.747×10^{-1}	-1.591×10^{-3}	1.750×10^{-6}	-7.523×10^{-10}	1.126×10^{-13}
2	0.319	-2.711×10^{-2}	8.393×10^{-4}	-9.044×10^{-7}	4.511×10^{-10}	-7.964×10^{-14}
3	2.808	-7.584×10^{-2}	5.586×10^{-4}	-5.761×10^{-8}	-1.575×10^{-10}	4.226×10^{-14}
4	26.235	4.024×10^{-1}	-8.570×10^{-6}	-4.818×10^{-7}	3.003×10^{-10}	-5.284×10^{-14}

Table 6 – WSGG model coefficients for H_2O at total pressure of 40 atm.

j	$\kappa_{p,j}$ (atm m)$^{-1}$	$b_{j,0}$	$b_{j,1}$ (K^{-1})	$b_{j,2}$ (K^{-2})	$b_{j,3}$ (K^{-3})	$b_{j,4}$ (K^{-4})
1	0.014	4.350×10^{-1}	-1.108×10^{-3}	1.354×10^{-6}	-6.439×10^{-10}	1.057×10^{-13}
2	0.132	4.570×10^{-1}	-5.952×10^{-4}	4.254×10^{-7}	-6.605×10^{-11}	-6.940×10^{-15}
3	1.018	-2.736×10^{-1}	9.947×10^{-4}	-4.444×10^{-7}	3.448×10^{-11}	7.893×10^{-15}
4	12.172	4.533×10^{-1}	3.093×10^{-4}	-7.827×10^{-7}	3.897×10^{-10}	-6.140×10^{-14}

In order to validate the obtained coefficients, total emittance values are calculated from the WSGG formulation on Eq. (8), compared to the LBL total emittance data which generated the coefficients in the first place, and the results are shown on Figs. 1 and 2 for both CO_2 and H_2O at total pressures of 1 atm, 10 atm, and 40 atm respectively. Figure 1

shows that for atmospheric pressure, both CO_2 and H_2O present good agreement between the results, implying that the WSGG coefficients provide a good fit of the LBL total emittance values. LBL emittance values look similar to the ones obtained by Cassol *et al*., 2014, for similar conditions, but the WSGG correlation for H_2O is better in the present work. For higher total pressure values the accuracy of the WSGG correlation reduces, especially for low path-length values of H_2O as shown on Fig. 2. However, these deviations at low path-lengths are not of major importance due to low radiative heat transfer in these cases, as stated by Cassol *et al*., 2014.

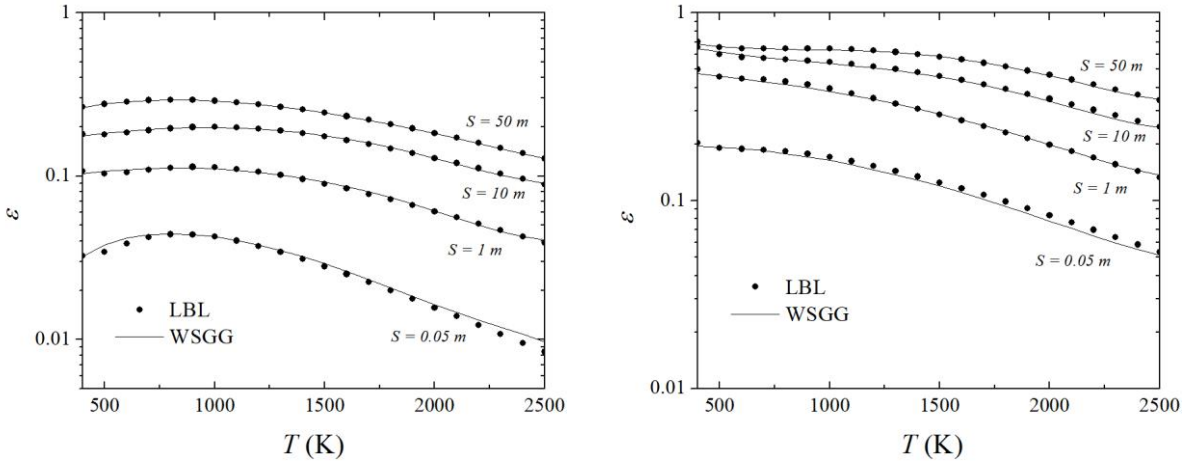

Figure 1 – Emittance as a function of temperature for total pressure of 1 atm calculated by LBL and WSGG for: (a) CO_2; (b) H_2O.

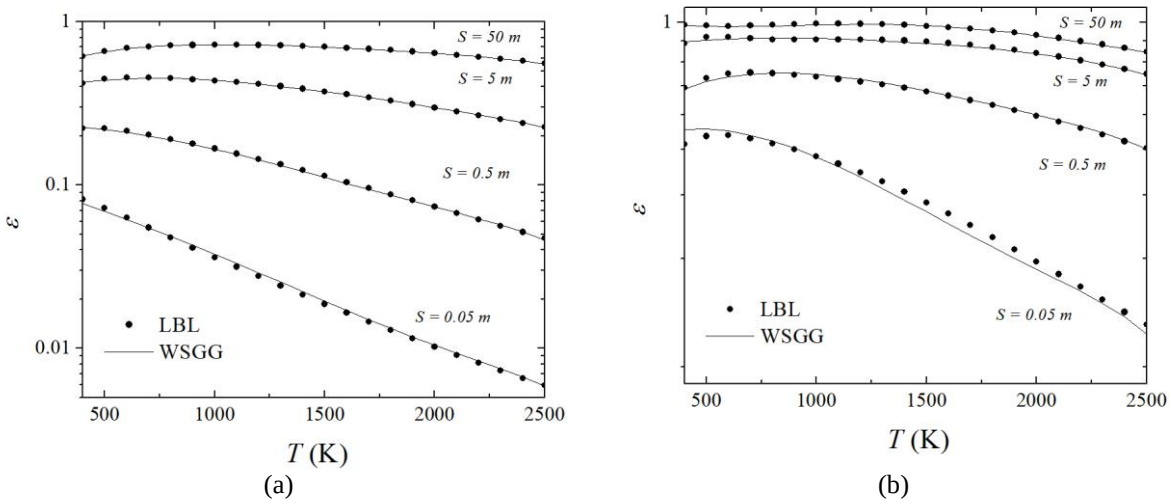

Figure 2 – Emittance as a function of temperature for total pressure of 40 atm calculated by LBL and WSGG for: (a) CO_2; (b) H_2O.

Comparing Figs. 1 and 2, it is noticeable that for the same path-lengths values total emittance increase considerably with total pressure for both species, showing the importance of accounting for the effect of pressure. This effect is even more important when analyzing radiative heat flux and heat source, as presented on Figs. 3 and 4 for the LBL results for CO_2 and H_2O respectively. According to the figures, both CO_2 and H_2O have very significant total pressure dependence on both radiative heat flux and heat source and this effect seems to attenuate as pressure increases. Figure 3 shows that radiative heat source on CO_2 has an increase on its maximum value of 111% from 1 atm to 10 atm and 183% from 1 atm to 40 atm while the radiative heat flux has an increase on its maximum value of 97% from 1 atm to 10 atm and 166% from 1 atm to 40 atm. In a similar way, Figure 4 shows that the radiative heat source on H_2O has an increase on its maximum value of 250% from 1 atm to 10 atm and 379% from 1 atm to 40 atm while the radiative heat flux has an increase on its maximum value of 167% from 1 atm to 10 atm and 212% from 1 atm to 40 atm. The attenuation of the total pressure effect is noticeable for higher pressures, which for CO_2 from 10 atm to 40 atm presents an increase of 34% on its maximum radiative heat source and 35% on its maximum radiative heat flux. However, for H_2O the

attenuation is even higher, which from 10 atm to 40 atm presents an increase of 37% on its maximum radiative heat source and 17% on its maximum radiative heat flux.

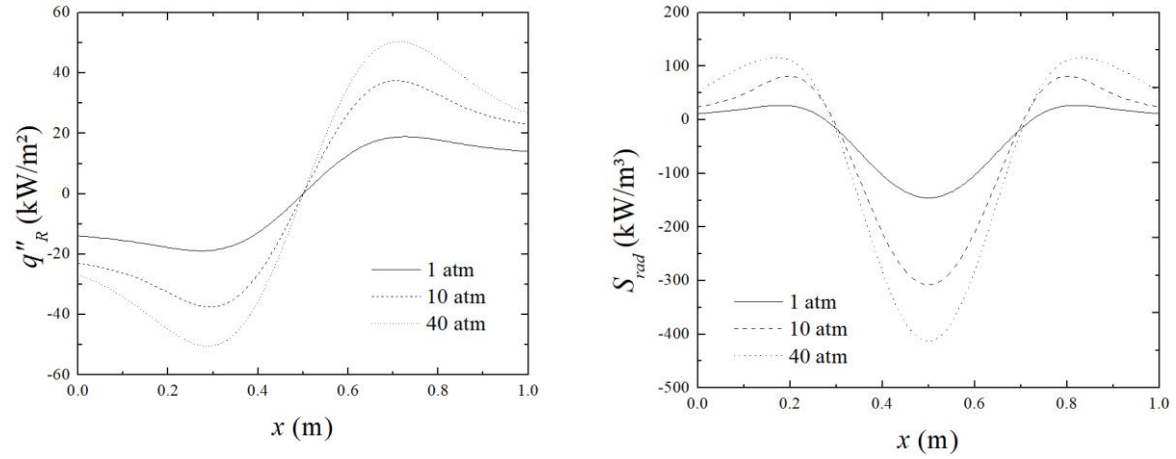

(a) (b)

Figure 3 – Total pressure effect on the LBL method results for CO_2: (a) radiative heat flux; (b) radiative heat source.

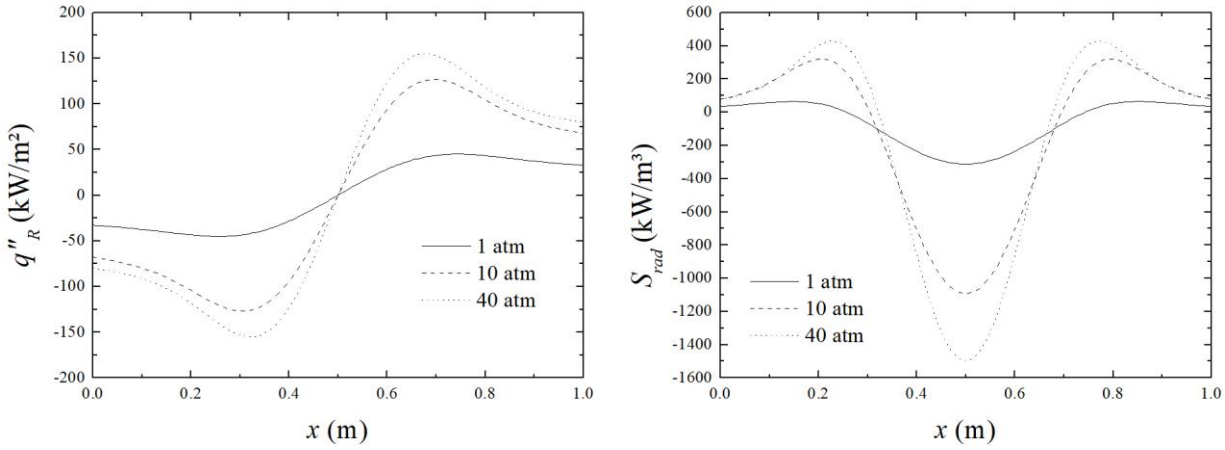

(a) (b)

Figure 4 – Total pressure effect on the LBL method results for H_2O: (a) radiative heat flux; (b) radiative heat source.

Figures 5, 6 and 7 present a comparison between the radiative heat flux and heat source calculated through the LBL and the WSGG for CO_2 at 1 atm, 10 atm, and 40 atm. Figures 5 and 6 show that both the radiative heat flux and heat source for pressures of 1 and 10 atm present larger deviations close to the wall. On the other hand, Figure 7 shows that for 40 atm the results from the WSGG method and the LBL are very close through the whole domain.

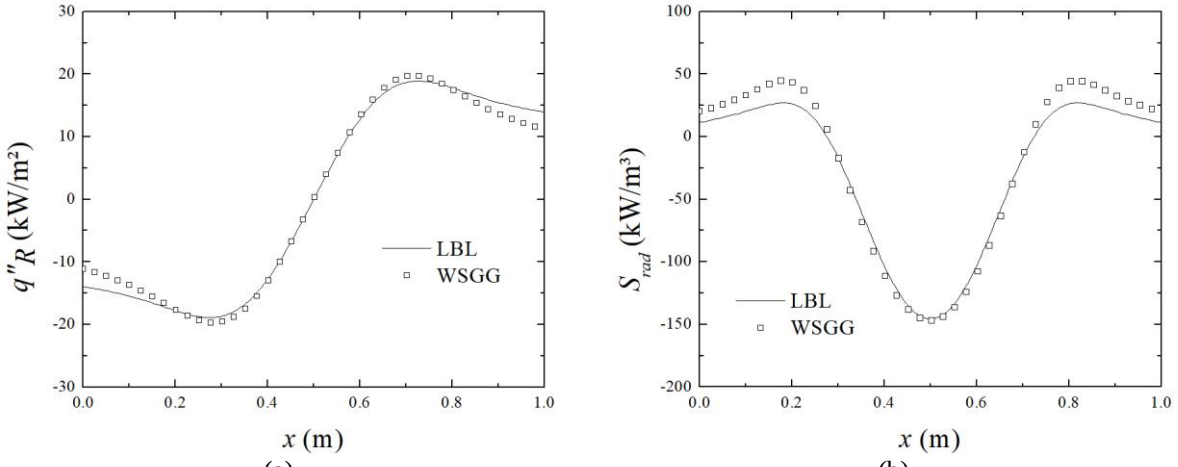

(a) (b)

Figure 5 – Results from the LBL and WSGG method for CO_2 at 1 atm for: (a) radiative heat flux; (b) radiative heat source.

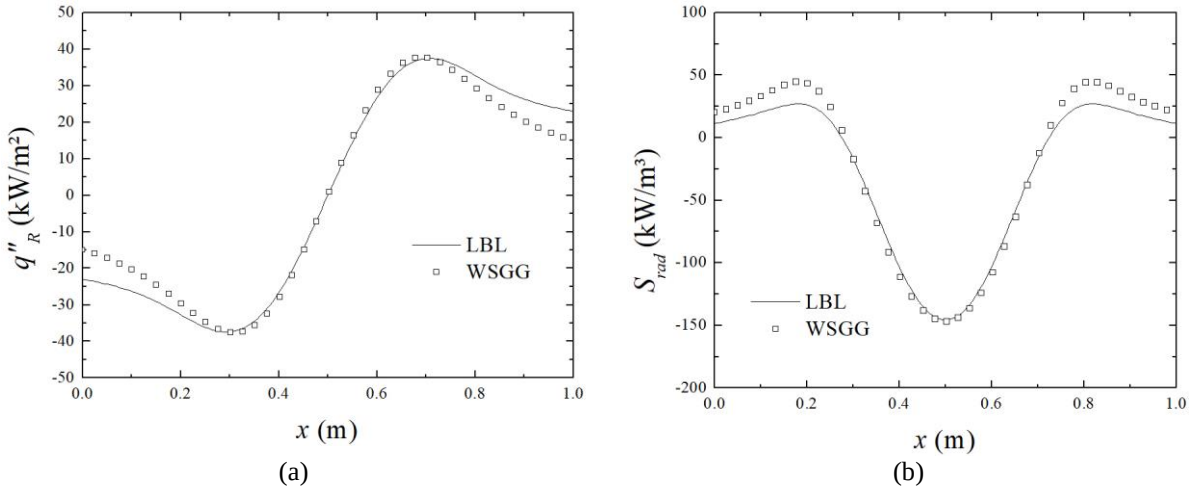

Figure 6 – Results from the LBL and WSGG method for CO_2 at 10 atm for: (a) radiative heat flux; (b) radiative heat source.

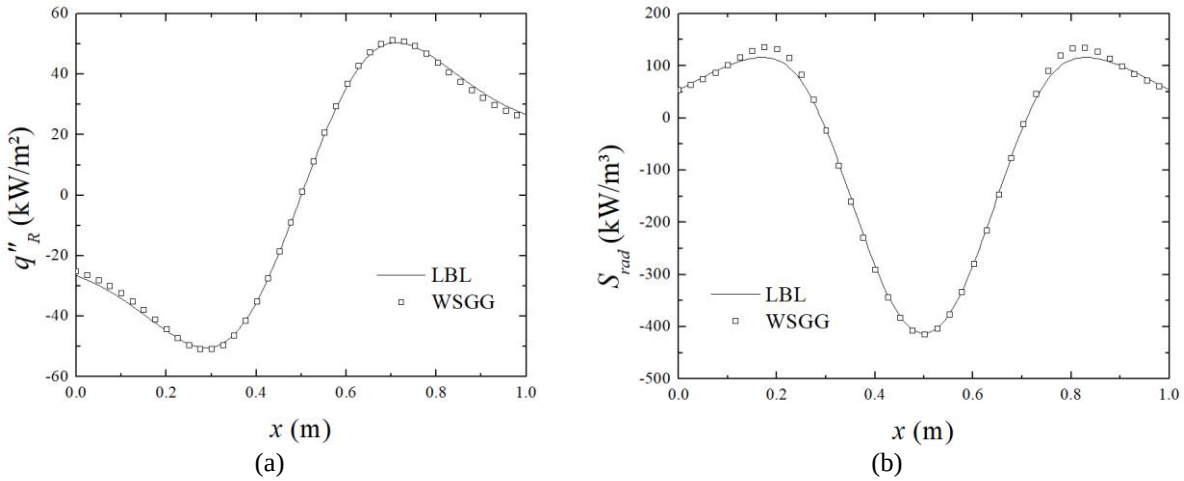

Figure 7 – Results from the LBL and WSGG method for CO_2 at 40 atm for: (a) radiative heat flux; (b) radiative heat source.

This behavior can also be noticed on Table 7 which presents the maximum and average deviations for the radiative heat flux and heat source obtained through the WSGG for CO_2 at pressures of 1 atm, 10 atm, and 40 atm. The values in the table show that the average deviations for WSGG are highest at 10 atm and lowest at 40 atm. This result is interesting because deviations for 40 atm are considerably lower than for atmospheric pressure which means the WSGG method has better performance on high pressure values for CO_2.

Table 7 – Radiative heat flux and heat source deviations for CO_2 at total pressures 1 atm, 10 atm, and 40 atm.

Total pressure (atm)	q''_R		S_R	
	δ_{max}(%)	δ_{med}(%)	ζ_{max}(%)	ζ_{med}(%)
1	14.83	5.08	12.11	6.34
10	21.36	8.23	11.39	7.33
40	3.59	1.69	5.10	1.73

Figures 8, 9 and 10 present a comparison between the radiative heat flux and heat source calculated through the LBL and the WSGG for H_2O at 1 atm, 10 atm, and 40 atm. Figure 8 shows that for atmospheric pressure the deviations of both the radiative heat flux and heat source increase with pressure. This behavior is the opposite from CO_2 which had better performance of the WSGG model for higher pressures. Also for H_2O this behavior looks smoother, increasing gradually as the pressure increases.

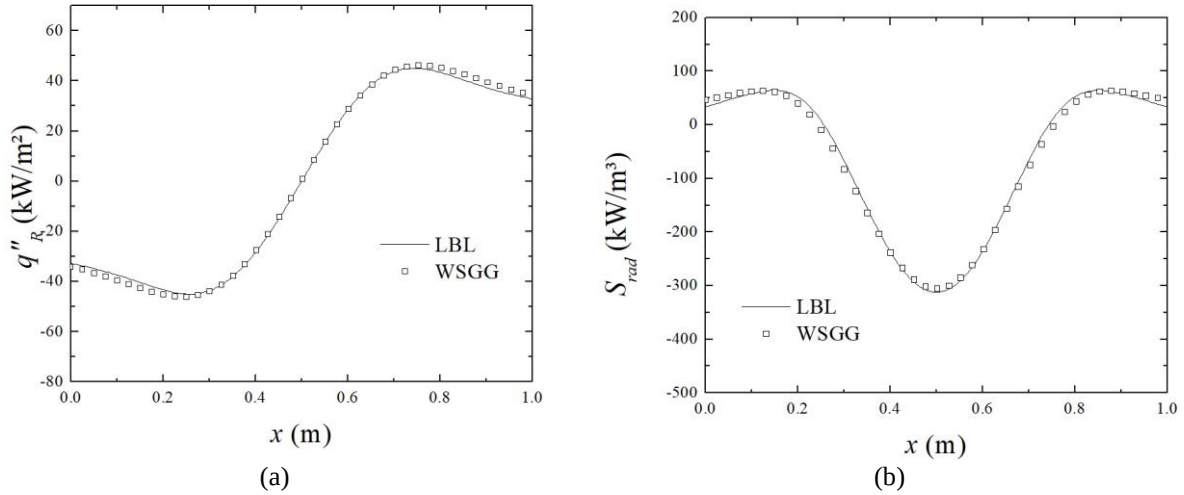

(a) (b)

Figure 8 – Results from the LBL and WSGG method for H_2O at 1 atm for: (a) radiative heat flux; (b) radiative heat source.

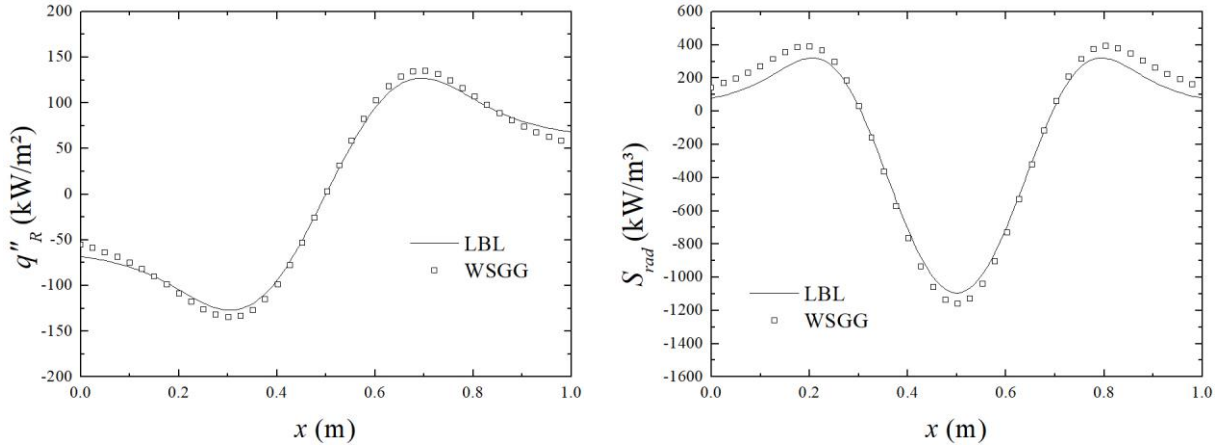

(a) (b)

Figure 9 – Results from the LBL and WSGG method for H_2O at 10 atm for: (a) radiative heat flux; (b) radiative heat source.

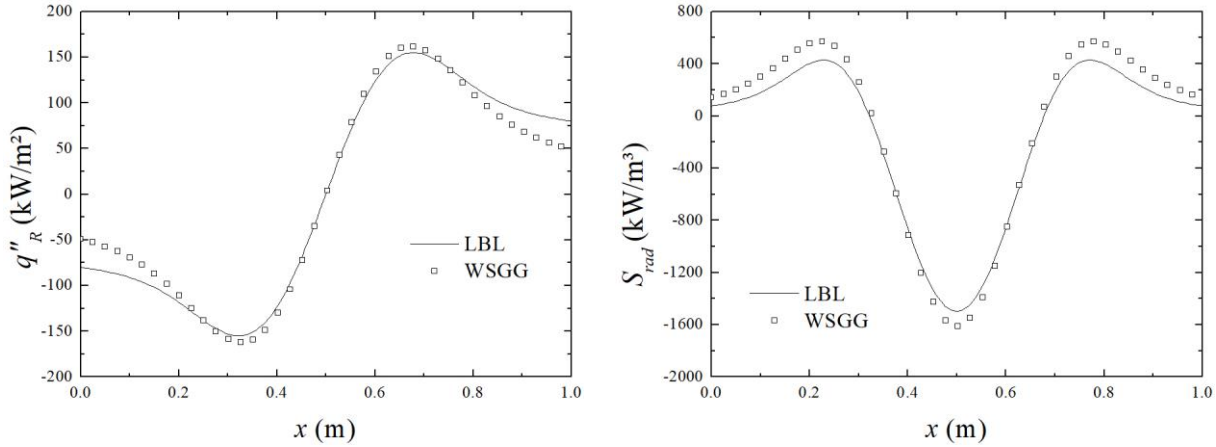

(a) (b)

Figure 10 – Results from the LBL and WSGG method for H_2O at 40 atm for: (a) radiative heat flux; (b) radiative heat source.

Table 8 presents the same pressure effect on maximum and average deviations for the radiative heat flux and heat source for H_2O at pressures of 1 atm, 10 atm, and 40 atm. The values in the table show that both the average deviations

and maximum deviations increase with pressure being lowest for 1 atm and highest for 40 atm. This result means the WSGG method has better performance on low pressure values for H_2O which is the opposite behavior as the one observed for CO_2. However, even for H_2O at 40 atm deviations are still acceptable, and are close to CO_2 at atmospheric pressure.

Table 8 – Radiative heat flux and heat source deviations for H_2O at total pressures 1 atm, 10 atm, and 40 atm.

Total pressure (atm)	$q_R^{"}$		S_R	
	δ_{max}	δ_{med}	ζ_{max}	ζ_{med}
1	5.04	2.50	5.42	2.57
10	10.07	4.59	8.57	5.31
40	20.07	7.60	10.40	6.49

Pearson et al., 2014, presents the effect of total pressure on the absorption cross-section of H_2O and CO_2 on similar conditions as this work, showing an attenuation of the absorption cross-section variation along the spectrum as the pressure increases for both species. This attenuation modifies the absorption spectrum in a way which the WSGG model might become more or less suitable to high pressures. According to the present work results, this attenuation makes the WSGG more suitable for CO_2 at higher total pressures while the opposite is observed for H_2O.

4. CONCLUSIONS

This work presented a methodology for generating WSGG coefficients applicable to high pressures, and was able to obtain new coefficients for CO_2 and H_2O that present good total emittance results for temperatures between 400 K and 2500 K and for total pressures of 1 atm, 10 atm, and 40 atm. The results of radiative heat flux and heat source were compared with the LBL solution, and the deviations between the solutions were acceptable, with average values below 10% for all cases. Finally, the effect of the total pressure was analyzed in all previous results, helping understand how total pressure influences thermal radiation of participating gases.

The total pressure effect was first noticeable on emittance results as emittance increased with pressure for same path-length values and for both species. This effect was even more important when analyzing radiative heat flux and heat source with both species presenting increases higher than 100% from 1 atm to 10 atm, and higher than 150% from 1 atm to 40 atm. However, the effect of pressure seems to attenuate as pressure increases for both species.

Another interesting result was the effect of pressure on the deviations of the radiative heat flux and heat source of the WSGG solution in comparison to the LBL. For CO_2 deviations were lowest at high pressure values, showing that the model developed in this work is suitable for high pressure CO_2 applications. The opposite was observed for H_2O, since all the deviations increased with pressure. A valid argument is that H_2O performs poorly at high pressures due to the greater number of spectral lines in its absorption spectrum. This result can also be related to the fact that H_2O has shown to be more sensitive to the effect of pressure in the LBL solution.

Even so, deviations for H_2O at 40 atm are not very different from those that other authors have already found for single species WSGG coefficients, and the method simplicity compensates for the lack of accuracy when compared to the LBL. Thus, it is concluded that the WSGG developed in this work is applicable for both CO_2 and H_2O under high pressure conditions, for molar fractions of $Y = 0.1$ and $Y = 0.2$ respectively, and temperatures ranging from 400 K to 2500 K.

5. ACKNOWLEDGEMENTS

Research developed with support from the Centro Nacional de Supercomputação (CESUP), Universidade Federal do Rio Grande (UFRGS).

6. REFERENCES

Alberti, M., Weber, R., Mancini, M., 2015. "Re-creating Hottel's emissivity charts for carbon dioxide and extending them to 40 bar pressure using HITEMP-2010 data base". Journal of Combustion and Flame, Vol. 162, p. 597–612.

Bordbar, M.H., Węcel, G., Hyppänen, T., 2014. "A line by line based weighted sum of gray gases model for inhomogeneous CO_2-H_2O mixture in oxy-fired combustion". Journal of Combustion and Flame, Vol. 161, p. 2435–2445.

Cassol, F., Brittes, R., França, F.H.R., Ezekoye, O.A., 2014. "Application of the weighted-sum-of-gray-gases model for media composed of arbitrary concentrations of H_2O, CO_2 and soot". International Journal of Heat and Mass Transfer, Vol. 79, p. 796-806.

Charest, M.R.J., Gülder, O.L., Groth, C.P.T., 2014. "Numerical and experimental study of soot formation in laminar diffusion flames burning simulated biogas fuels at elevated pressures". Journal of Combustion and Flame, Vol. 161, p. 2678-2691.

Chu, H., Gu, M., Consalvi, J.L., Liu, F., 2016. "Effects of total pressure on non-grey gas radiation transfer in oxy-fuel combustion using the LBL, SNB, SNBCK, WSGG and FSCK methods". Journal of Quantitative Spectroscopy & Radiative Transfer, Vol. 172, p. 24–35.

Dorigon, L.J., Duciak, G., Brittes, R. Cassol, F. Galarça, M. and França, F.H.R., 2013. "WSGG correlations based on HITEMP 2010 for computation of thermal radiation in non-isothermal, non-homogeneous H_2O/CO_2 mixtures". International Journal of Heat and Mass Transfer, Vol. 64, p. 863–873.

Hottel, H.C. and Sarofim, A.F., 1967. Radiation Transfer. McGraw-Hill, New York.

Kangwanpongpan, T., França, F.H.R., da Silva, R.C., Schneider, P.S., Krautz, H.J., 2012. "New correlations for the weighted-sum-of-gray-gases model in oxy-fuel conditions based on HITEMP 2010 database". International Journal of Heat and Mass Transfer, Vol. 55, p. 7419-7433.

Kez, V., Liu, F., Consalvi, J.L., Ströhle, J., Epple, B., 2016. "A comprehensive evaluation of different radiation models in a gas turbine combustor under conditions of oxy-fuel combustion with dry recycle". Journal of Quantitative Spectroscopy & Radiative Transfer, Vol. 172, p. 121–133.

Matynia, A., Idir, M., Molet, J., Roche, S., Persis, S., Pillier, L., 2012. "Absolute OH concentration profiles measurements in high pressure counterflow flames by coupling LIF, PLIF, and absorption techniques". Applied Physics B, Vol. 108, p. 393-405.

Siegel, R. and Howell, J., 2002. Thermal Radiation Heat transfer. Taylor and Francis, New York, 4th edition.

Pearson, J.T., Webb, B.W, Solovjov, V.P., Ma, J., 2014. "Effect of total pressure on the absorption line blackbody distribution function and radiative transfer in H_2O, CO_2, and CO". Journal of Quantitative Spectroscopy & Radiative Transfer, Vol. 143, p. 100–110.

Rothman, L.S., Gordon, I.E., Barber, R.J., Dothe, H., Gamache, R.R., Goldman, A., Perevalov, V.I., Tashkun, S.A., Tennyson, J., 2010. "HITEMP, the high-temperature molecular spectroscopic database". Journal of Quantitative Spectroscopy & Radiative Transfer, Vol. 111, p. 2139-2150.

Smith, T.F., Shen, Z.F., Friedman, J.N., 1982. "Evaluation of coefficients for the weighted sum of gray gases model". Journal of Heat Transfer, Vol. 104, p. 602-608.

7. RESPONSIBILITY NOTICE

The authors are the only responsible for the printed material included in this paper.